In Vitro Heavy-Atom Effect of Palladium(II) and Platinum(II) Complexes of Pyrrolidine-Fused Chlorin in Photodynamic Therapy

Makoto Obata,*[,†] Shiho Hirohara,*[,‡] Rika Tanaka,[§] Isamu Kinoshita,[||] Kei Ohkubo,[⊥] Shunichi Fukuzumi,[⊥] Masao Tanihara,[‡] and Shigenobu Yano*[,#]

Graduate School of Humanities and Sciences, Nara Women's University, Kitauoyanishimachi, Nara 630-8506, Japan, Graduate School of Materials Science, Nara Institute of Science and Technology, Takayama 8916-5, Ikoma, Nara 630-0192, Japan, Graduate School of Engineering, Osaka City University, Osaka 577-8502, Japan, Departments of Molecular Materials Science, Graduate School of Science, Osaka City University, Osaka 577-8502, Japan, Department of Material and Life Science, Graduate School of Engineering, Osaka University, SORST, Japan Science and Technology Agency, Suita, Osaka 565-0871, Japan, Endowed Research Section, Photomedical Science, Innovative Collaboration Center, Kyoto University, Kyoto-daigaku Katsura, Nishikyo-ku, Kyoto 615-8520, Japan

Received December 7, 2008

Introduction of a heavy atom into photosensitizers generally facilitates intersystem crossing and improves the quantum yield (Φ_Δ) of singlet oxygen ($^1O_2$), which is a key species in photodynamic therapy (PDT). However, little information is available about the physiological importance of this heavy-atom effect. The aim of this study is to examine the heavy-atom effect in simple metallochlorins in vitro at the cellular level. 1,3-Dipolar cycloaddition of azomethine ylide to 5,10,15,20-tetrakis(pentafluorophenyl)porphyrinato palladium(II) and platinum(II) afforded metallochlorins **4b** and **4c** in yields of 17.1 and 12.9%, respectively. The Φ_Δ values increased in the order of **4a** (0.28) < **4b** (0.89) < **4c** (0.92) in C_6D_6. The photocytotoxicity of **4a**, **4b**, and **4c** was evaluated in HeLa cells at a light dose of 16 J·cm^{-2} with $\lambda > 500$ nm and increased in the order of **4a** < **4b** < **4c** at the concentration of 0.5 μM. The photocytotoxicity of **4b** and **4c** was significantly inhibited by addition of sodium azide, but not D-mannitol, suggesting that $^1O_2$ is the major species causing cell death. Our results clearly indicate that **4b** and **4c** act as efficient $^1O_2$ generators due to the heavy-atom effect in a cellular microenvironment as well as in nonphysiological media.

Introduction

Photodynamic therapy (PDT) with a photosensitizer and light irradiation results in lethal photochemical reactions in cells and is used to treat tumors.[1−6] The mechanism of PDT has been well studied,[4,7−9] and the physicochemical and biological requirements for PDT photosensitizers have become clear. One of the crucial requirements is light-absorbing ability in the so-called PDT window, in the wavelength range from 600 to 800 nm, which affords good light penetration into tissues and an appropriate energy to activate oxygen molecules.[7] The initial work on hematoporphyrin derivatives[3] has let to further studies of possible second-generation photosensitizers such as chlorins and bacteriochlorins. It is important that the oxygen molecule should reach the singlet excited state through efficient energy transfer from an excited triplet state of the photosensitizer. Intersystem crossing between singlet and triplet states is generally promoted by spin−orbit coupling, which increases as a function of Z^4 (Z is atomic number).[10] Introduction of heavy metal ions into a photosensitizer therefore results in an improvement of the singlet oxygen ($^1O_2$) quantum yield. Hence, metal complexes of hydroporphyrin derivatives are considered an interesting design for PDT photosensitizers.[11]

Chart 1. Metal Complexes for PDT Photosensitizers

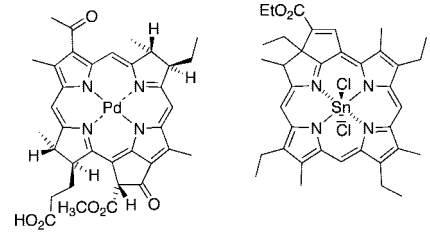

1 **2**

Chlorophylls and bacteriochlorophylls are naturally occurring metal (typically magnesium or zinc) complexes of hydroporphyrins. Not only native pigments, but also chemically modified ones, have been examined as candidate photosensitizers for PDT.[12−16] Recently Salomon and Scherz have developed a palladium(II) complex of bacteriopheophorbide **1** (Chart 1) and is currently under clinical trial for treating prostate cancer.[17,18] The introduction of palladium(II) ion improves the photostability of bacteriopheophorbide and results in a high yield of $^1O_2$ (~100% in organic solvent).[18] The tin complex of etiopurpurin **2** is also promising photosensitizer with a $^1O_2$ quantum yield of 0.71 ± 0.1 in acetonitrile[19] and is under clinical trial for the treatment of wet age-related macular degeneration. Metal complexes of fully synthetic hydroporphyrins have also been intensively studied, especially as models of naturally occurring pigments and enzyme active sites.[20−23] To our knowledge, however, none of them has have been applied in PDT treatment.

Acceleration of intersystem crossing by the introduction of a heavy atoms is well established and frequently utilized in PDT photosensitizers.[24−27] However, so far there is little evidence that this results in an improved systematic cellular response in vitro. For example, Serra et al. examined the effect of halogena-

* To whom correspondence should be addressed. For M.O.: phone, +81 742203622; fax, +81 742203622; E-mail, mobata@cc.nara-wu.ac.jp. For S.H.: phone, +81 743726122; fax, +81 743726129; E-mail, hirohara@ms.naist.jp. For S.Y.: phone, +81 75383072; fax, +81 753833072; E-mail, yano@icc.kyoto-u.ac.jp.
† Nara Women's University.
‡ Nara Institute of Science and Technology.
§ Graduate School of Engineering, Osaka City University.
|| Graduate School of Science, Osaka City University.
⊥ Osaka University.
Kyoto University.

10.1021/jm8015427 CCC: $40.75
Published on Web 04/20/2009

Scheme 1

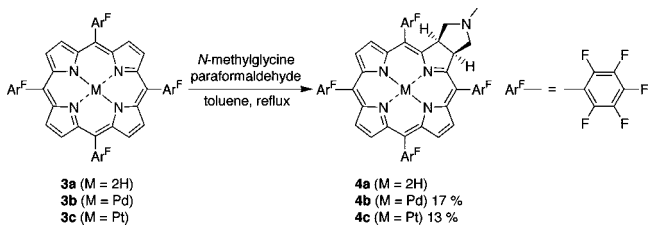

tion of 5,10,15,20-tetrakis(3-hydroxyphenyl)porphyrin on the $^1O_2$ quantum yield as well as in vitro photocytotoxicity in WiDr human colon adenocarcinoma cells and melanoma A375 cells.[28] They found a small improvement (from 0.50 to 0.55 or 0.58) in the $^1O_2$ quantum yield by introducing bromine or iodine into the peripheral phenyl groups. However, there was no clear heavy-atom effect on the photodynamic action. The introduction of bromine increased the photocytotoxicity, but iodinated photosensitizers showed weaker photocytotoxicity than the nonhalogenated compounds. Presumably the effect of the heavy atom was masked by changes in lipophilicity and cellular uptake. In the case of nontetrapyrrolic photosensitizers, Gorman et al. synthesized azadipyrromethane-based photosensitizers having bromine at various positions.[29] The $^1O_2$ quantum yields of these photosensitizers depended on the distance between the chromophore and bromine atom. In addition, the in vitro photocytotoxicities in MRC5-SV40-transformed fibroblast cells and HeLa cells were consistent with those expected based on the heavy-atom effect. However, there have been no systematic studies on the in vitro heavy-atom effect in metal complexes of fully synthetic hydroporphyrins.

To examine the in vitro heavy-atom effect in metal complexes of fully synthetic hydroporphyrins, we synthesized two metallochlorins, i.e., the palladium(II) ($Z = 46$) and platinum(II) ($Z = 78$) complexes denoted as **4b** and **4c**, respectively, in Scheme 1. In this paper, we report the synthesis of **4b** and **4c**, confirmation of the structures by X-ray crystallography, and an evaluation of the physicochemical properties and in vitro photocytotoxicity to HeLa cells of these complexes.

Results and Discussion

Chemistry. 1,3-Dipolar cycloaddition of azomethine ylide is powerful tool to synthesize chlorins from electron-deficient porphyrin.[30−32] To our knowledge, however, 1,3-dipolar cycloaddition of metalloporphyrin has not been reported.[33] To synthesize metallochlorins, we adopted the cycloaddition to 5,10,15,20-tetrakis(pentafluorophenyl)porphyrin (**3a**) and its palladium(II) and platinum(II) metal complexes (**3b** and **3c**). **3a**, **3b**, and **3c** were prepared according to the literatures.[34−36] 1,3-Dipolar cycloadditions of **3a**, **3b**, and **3c** with azomethine ylide were conducted in toluene using *N*-methylglycine and paraformaldehyde (Scheme 1).[30] The crude products were purified by silica gel column chromatography followed by gel permeation chromatography. The resulting chlorins **4a**, **4b**, and **4c** were characterized by ^1H, ^{13}C, and ^{19}F NMR spectroscopies, UV−vis and IR spectroscopies, and elemental analysis. The ^1H and ^{19}F NMR spectra of **4a**, **4b**, and **4c** clearly indicated C_S symmetry of the molecules. The intense ^{19}F NMR signals are interesting in the light of recent developments in ^{19}F MRI applications.[37] Metallochlorins **4b** and **4c** afforded single crystals suitable for X-ray crystallography from a mixture of CH_2Cl_2 and hexane. The crystal structure of **4b** was essentially identical to that of **4c**. Figure 1 shows the crystal structure of **4c**, and Table 1 lists selected bond lengths and angles for **4b** and **4c**.

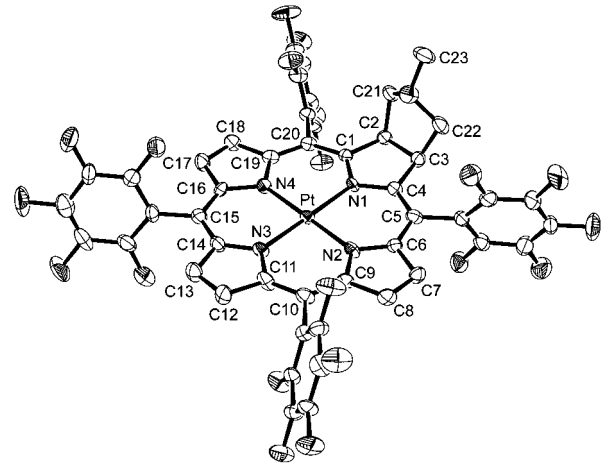

Figure 1. ORTEP drawing of **4c** with thermal ellipsoids shown at the 50% probability level. Hexane molecule and hydrogen atoms are omitted for clarity.

Table 1. Selected Bond Lengths (in Å) and Angles (deg) for Metallochlorins **4b** and **4c**

parameter		**4b**	**4c**
M−N(pyrroline)	M−N(1)	2.050(4)	2.052(6)
M−N(pyrrole)	M−N(2)	2.021(4)	2.025(6)
	M−N(3)	2.033(4)	2.048(6)
	M−N(4)	2.010(4)	2.027(6)
$C_\alpha-C_\beta$ in pyrroline	C(1)−C(2)	1.516(7)	1.522(11)
	C(3)−C(4)	1.510(6)	1.521(10)
$C_\beta-C_\beta$ in pyrroline	C(2)−C(3)	1.532(7)	1.540(11)
$C_\alpha-C_\beta$ in pyrrole B	C(6)−C(7)	1.451(7)	1.440(11)
	C(8)−C(9)	1.432(7)	1.434(11)
$C_\beta-C_\beta$ in pyrrole B	C(7)−C(8)	1.330(7)	1.341(11)
$C_\alpha-C_\beta$ in pyrrole C	C(11)−N(12)	1.430(7)	1.445(11)
	C(13)−C(C14)	1.439(7)	1.439(11)
$C_\beta-C_\beta$ in pyrrole C	C(12)−C(13)	1.347(8)	1.351(13)
$C_\alpha-C_\beta$ in pyrrole D	C(16)−C(17)	1.425(7)	1.439(11)
	C(18)−C(19)	1.446(7)	1.444(11)
$C_\beta-C_\beta$ in pyrrole D	C(17)−C(18)	1.348(7)	1.344(11)
$C_\alpha-M-C_\alpha$ in pyrroline	C(1)−N(1)−C(4)	108.5(4)	109.2(6)
$C_\alpha-M-C_\alpha$ in pyrrole B	C(6)−N(2)−C(9)	106.6(4)	105.6(6)
$C_\alpha-M-C_\alpha$ in pyrrole C	C(11)−N(3)−C(14)	106.1(4)	107.6(6)
$C_\alpha-M-C_\alpha$ in pyrrole D	C(16)−N(4)−C(19)	105.2(4)	105.5(6)

The *N*-methylpyrrolidine ring takes an envelope conformation, with C_S symmetry, in which the chlorin ring has exo configuration with regard to the methyl group. The configuration of *N*-methylpyrrolidine is the same as that of locked *meso*-β-substituted chlorins.[32] The bond distances between palladium(II) or platinum(II) and pyrroline nitrogen were found to be 2.050(4) and 2.052(6) Å, which are slightly longer than those between metal ion and pyrrole nitrogen. Similar but clearer trends were reported in zinc(II),[38,39] iron(II),[40] and nickel(II)[41,42] complexes of hydroporphyrins. The $C_\beta-C_\beta$ bond of the pyrroline ring (1.532(7) and 1.540(11) Å for **4b** and **4c**, respectively) is remarkably longer than those of the pyrrole rings (average lengths of 1.342 and 1.345 Å for **4b** and **4c**, respectively). The average deviation from the mean plane of the chlorin ring (20 carbons and 4 nitrogens) and metal ion was calculated to be 0.034 and 0.033 Å for **4b** and **4c**, respectively. Hence, the chlorin rings of **4b** and **4c** have substantially planar structures, like **3c** (0.006 Å).[36] Stolzenberg et al. also reported that the palladium(II) complexes of *trans*-octaethylchlorin and *tct*-octaethylisobacteriochlorin have planar structures.[43] Usually, metal complexes of hydroporphyrins deform from planar to S_4 ruffled or domed conformation due to the low conjugation energy. For example, nickel(II) complexes of chlorin[41] and isobacteriochlorin[42] showed great deviation from planar structure

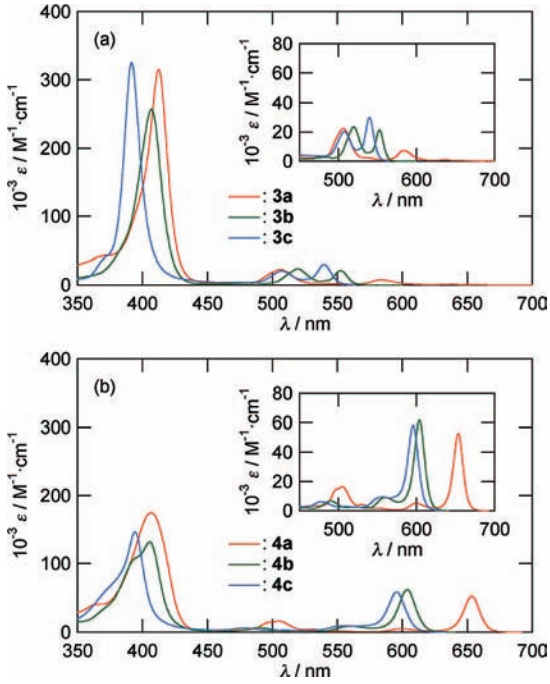

Figure 2. UV−vis spectra of porphyrins (**3a**, **3b**, and **3c**) (a) and chlorins (**4a**, **4b**, and **4c**) (b) in $CHCl_3$ at 25 °C.

Table 2. Spectral Data of Porphyrins (**3a**, **3b**, and **3c**) and Chlorins (**4a**, **4b**, and **4c**) in $CHCl_3$ at 25 °C.

	λ_{max}/nm ($10^{-3}\varepsilon$/M^{-1}·cm^{-1})				
	Soret band	Q bands			
3a	413 (315)	507 (22.4)	538 (2.40)	583 (7.22)	638 (1.07)
3b	407 (257)	520 (23.5)	553 (21.3)		
3c	392 (325)	508 (20.4)	540 (29.9)		
4a	407 (175)	505 (16.5)	599 (5.15)	654 (52.7)	
4b	406 (132)	490 (6.66)	561 (9.02)	604 (61.5)	
4c	395 (147)	478 (6.03)	557 (9.33)	596 (58.0)	

because the preferred bond length between nickel(II) and nitrogen (ca. 1.85 Å) is shorter than the porphyrin pore size (ca. 1.99 Å). On the other hand, typical bond lengths between palladium(II) or platinum(II) and nitrogen are ca. 2.00 Å, which fits the porphyrin pore. This favors retention of the planar structure of **4b** and **4c**. This structural feature is important in the design of PDT photosensitizers having enhanced singlet oxygen ($^1O_2$) generation due to the heavy-atom effect because S_4 ruffled structure sometimes facilitates nonradiative deactivation of the excited triplet state, reducing the $^1O_2$ quantum yield.[44,45] The pentafluorophenyl (Ar^F) rings of **4b** and **4c** were significantly inclined from the perpendicular position to the chlorin rings, unlike those in **3c**.[36] The angles between the mean planes of chlorin and the 10- and 15-Ar^F rings were 69.54° and 71.82° for **4b** and 69.69° and 71.67° for **4c**. On the other hand, the angles for the 5- and 20-Ar^F rings were much closer to perpendicular: 83.46° and 78.45° for **4b** and 83.23° and 78.31° for **4c**. The crystal packing indicated the presence of C−H···F type interaction[46] between fluorine of the pentafluorophenyl rings and the methyl and methylene protons in the *N*-methylpyrrolidine ring of neighboring molecules, resulting in distorted conformation of the pentafluorophenyl rings with respect to the chlorin ring.

Figure 2 shows UV−vis spectra of porphyrins **3a**, **3b**, and **3c** and chlorins **4a**, **4b**, and **4c** in $CHCl_3$ at 25 °C, and Table 2 summarizes the spectral data. The fluorination of the phenyl groups resulted in a small hypsochromic shift of the Soret and Q bands for free-base porphyrin but had substantially no effect

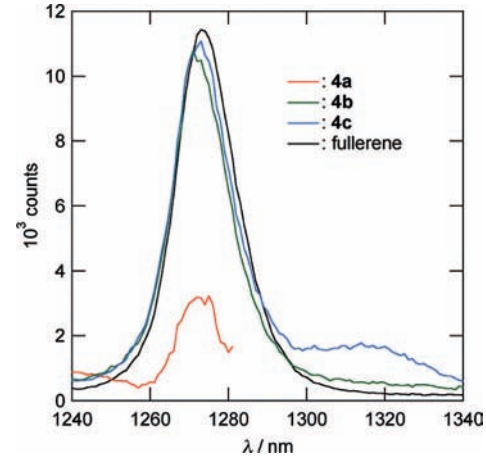

Figure 3. Luminescence spectra of $^1O_2$ generated by photosensitization using **4a**, **4b**, **4c**, and fullerene in C_6D_6. The large peak due to fluorescence of **4a**, which was found at ca. 1320 nm, were omitted for clarity.

for the palladium(II) and platinum(II) complexes. On the other hand, the introduction of palladium(II) and platinum(II) ions brings about a significant hypsochromic shift, which is a major drawback to using metal complexes of porphyrins as PDT photosensitizers. The 1,3-dipolar cycloaddition of azomethine ylide on porphyrins resulted in batho- and hyperchromic effects on the Q bands in metallochlorins. The resulting (metallo)chlorins showed an intense Q_I band, with ε_{max} values of more than 5×10^4 M^{-1}·cm^{-1} at 654, 604, and 596 nm for **4a**, **4b**, and **4c**, respectively. The λ_{max} and ε_{max} values of **4a** are comparable to those of 5,10,15,20-tetrakis(3-hydroxyphenyl)chlorin. Even though introduction of palladium(II) and platinum(II) ions leads a significant hypsochromic shift (ca. 50 nm), thanks to 1,3-dipolar cycloaddition, the metallochlorins **4b** and **4c** still have an PDT-applicable absorption around 600 nm.

Singlet oxygen ($^1O_2$), which is thought to be a primary cytotoxic species in photodynamic therapy, was detected by making use of the $^1O_2$ luminescence at 1270 nm in O_2-saturated C_6D_6 (Figure 3). The $^1O_2$ quantum yields (Φ_Δ) were determined to be 0.28, 0.89, and 0.92 for **4a**, **4b**, and **4c**, respectively, using fullerene ($\Phi_\Delta = 0.96$)[47] as a standard. While **4a** showed a relatively small Φ_Δ value, its palladium(II) and platinum(II) complexes were found to be excellent $^1O_2$ generators in organic solvents owing to the heavy-atom effect.[11]

Biology. Dark cytotoxicity and photocytotoxicity of porphyrins (**3a**, **3b**, and **3c**) and chlorins (**4a**, **4b** and **4c**) were tested in HeLa cells using a 100 W halogen lamp equipped with sharp-cut filter ($\lambda > 500$ nm) as a light source. HeLa cells (5×10^3 cells/well) were incubated with photosensitizers for 24 h and photoirradiated with a predetermined light dose (0 or 16 J·cm^{-2} for dark cytotoxicity and photocytotoxicity tests, respectively). After 24 h photoirradiation, the survival rate was estimated in terms of the mitochondrial activity of NADH dehydrogenase using WST-8 assay. Figure 4 shows the dark cytotoxicity and photocytotoxicity of **3a**, **3b**, **3c**, **4a**, **4b**, and **4c** at the concentration of 5 μM. None of the photosensitizers tested showed dark cytotoxicity under these conditions. Upon photoirradiation, chlorins **4a**, **4b** and **4c** killed almost all of the cells, while porphyrins showed no photocytotoxicity under the same conditions, possibly due to their poor light-absorbing properties. Metallochlorins **4b** and **4c** retained appreciable photocytotoxicity even at the low concentration of 0.5 μM (Figure 5), while **4a** showed almost no photocytotoxicity at this concentration The order of photocytotoxicity was found to be **4a** < **4b** < **4c**, which

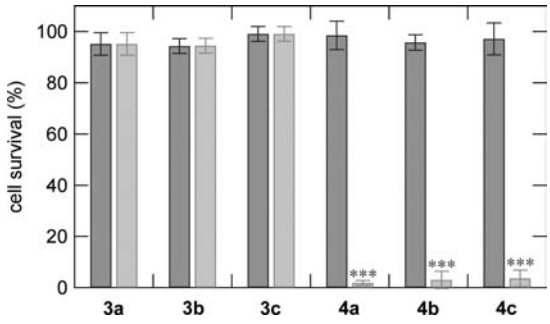

Figure 4. Cytotoxicity in the dark (left bar) and photocytotoxicity (right bar) of porphyrins (**3a**, **3b**, and **3c**) and chlorins (**4a**, **4b**, and **4c**) in HeLa cells. The drug concentration was 5 μM. The light dose was 16 J·cm^{-2} from a 100 W halogen lamp (λ > 500 nm). The percentage cell survival was determined by WST-8 assay at 24 h after photoirradiation. The values represent the means ± standard deviations of six replicate experiments. ***Significant difference, p < 0.001 vs dark cytotoxicity.

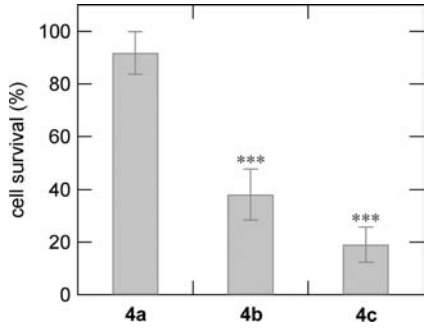

Figure 5. Photocytotoxicity of chlorins (**4a**, **4b**, and **4c**) in HeLa cells. The drug concentration was 0.5 μM. The light dose was 16 J·cm^{-2} from a 100 W halogen lamp (λ > 500 nm). The percentage cell survival was determined by WST-8 assay at 24 h after photoirradiation. The values represent the means ± standard deviations of six replicate experiments. ***Significant difference, p < 0.001 vs **4a**.

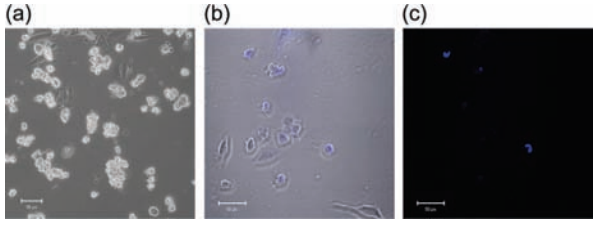

Figure 6. HeLa cells treated with **4c** and photoirradiation. Bright field image (a) of HeLa cells at 3 h after photoirradiation, and bright field (b) and fluorescent (c) images of DAPI-stained HeLa cells at 24 h after photoirradiation. Excitation wavelength was 364 nm (b) or 543 nm (c).

is consistent with the order of the Φ_Δ values, suggesting that $^1O_2$ is a key species in photodynamic action (vide infra). The bright field image of HeLa cells treated with **4c** (0.5 μM) and photoirradiated 3 h clearly showed shrunken and spherical cells with apoptotic bodies (Figure 6). In addition, DAPI-stained HeLa cells emitted strong blue luminescence, indicating chromatin condensation after 24 h photoirradiation. These morphological changes show that photoirradiation in the presence of **4c** initiated an apoptotic process.

Photocytotoxicity is thought to be a consequence of oxidative stress induced by reactive oxygen species (ROS). The kind of ROS involved depends on the type of photoreaction, namely hydrogen or electron transfer reaction (type I photoreaction) or energy transfer reaction (type II photoreaction). Type I photo-

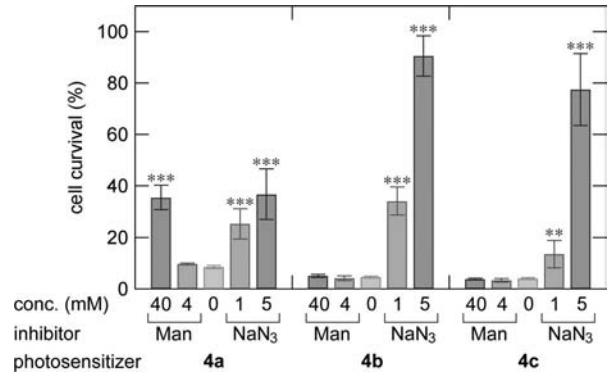

Figure 7. Cell survival (%) of HeLa cells treated with **4a** (0.8 μM), **4b** (0.4 μM), and **4c** (0.4 μM) in the absence of ROS quenchers and in the presence of 1 and 5 mM sodium azide (NaN_3, $^1O_2$ quencher) and 4 and 40 mM D-mannitol (Man, •OH radical scavenger). The light dose was 16 J·cm^{-2} from a 100 W halogen lamp (λ > 500 nm). The percentage cell survival was determined by WST-8 assay at 24 h after photoirradiation. The values represent the means ± standard deviations of six replicate experiments. ***Significant difference, p < 0.001 vs no ROS quenchers. **Significant difference, p < 0.01 vs no ROS quenchers.

reaction takes place between the excited photosensitizer and a substrate such as water, to form hydroxyl radical (OH•) and superoxide anion (O_2^-). On the other hand, type II photoreaction between excited photosensitizers and molecular oxygen ($^3O_2$) generates highly reactive $^1O_2$. $^1O_2$ is usually thought to be the dominant photocytotoxic species because of its relatively long lifetime. As already mentioned, **4a**, **4b**, and **4c** generate $^1O_2$ in organic media (C_6D_6). Scherz et al. tested the microenvironmental effect on the generation of ROS in palladium(II) complex of bacteriopheophorbide **1**.[18] They found that **1** generates ROS in a medium-dependent fashion, and the electron-transfer reaction is increased in polar media. Hence, the kind of ROS involved in HeLa cells killing may be different from that generated in an organic medium. In this regard, Gu et al. tested the photocytotoxicity of hematoporphyrin monomethyl ester in the presence of ROS inhibitors, namely sodium azide as an $^1O_2$ quencher and D-mannitol as an OH• scavenger.[48] They found significant inhibition of photocytotoxicity by both sodium azide and D-mannitol and concluded that hematoporphyrin monomethyl ester formed both $^1O_2$ and OH• through type I and type II reactions, respectively. To determine which ROS is predominantly involved in cell death, we used a modification of Gu's procedure to examine the photocytotoxicity of **4a**, **4b** and **4c** to HeLa cells in the presence of sodium azide and D-mannitol. Figure 7 shows dose-dependent inhibitory effects of D-mannitol (4 and 40 mM) and sodium azide (1 and 5 mM) on the photocytotoxicity of **4a** in HeLa cells. On the other hand, the photocytotoxicities of **4b** and **4c** were quenched by 5 mM sodium azide but not by 40 mM D-mannitol. In the case of **4b** and **4c**, therefore, $^1O_2$ formed by energy transfer is dominantly responsible for photocytotoxicity to HeLa cells, whereas other species besides singlet oxygen could be participate in the photocytotoxicity of **4a**. The photocytotoxicity induced by **4a** is similar to that of hematoporphyrin monomethyl ether,[48] indicating that both $^1O_2$ and OH• can cause cell death. This is consistent with the poor $^1O_2$ quantum yield of **4a** in organic media. On the other hand, **4b** and **4c** generate $^1O_2$ efficiently in the cellular microenvironment as well as in organic media. These

results demonstrate that there is a heavy-atom effect in hydroporphyrin at the cellular level in vitro.

Conclusion

Novel palladium(II) and platinum(II) complexes of chlorins (**4b** and **4c**, respectively) were prepared by 1,3-dipolar cycloaddition of the corresponding palladium(II) and platinum(II) complexes of tetrakis(pentafluorophenyl)porphyrin (**4b** and **4c**, respectively). The structures of **4b** and **4c** were fully characterized by X-ray crystallography. The chlorin rings of **4b** and **4c** have a planar structure because the typical Pd(II)−N and Pt(II)−N bond distances are consistent with the chlorin ring dimensions. The $^1O_2$ quantum yields of **4a**, **4b**, and **4c** in C_6D_6 were determined by luminescence measurement of $^1O_2$ and increased in the order of **4a** < **4b** < **4c**. The improvement of $^1O_2$ quantum yield can be attributed to the heavy-atom effect of palladium(II) or platinum(II) ions, which is well established in nonphysiological media. Pyrrolidine-fused chlorins **4a**, **4b**, and **4c** showed remarkable photocytotoxicity in HeLa cells at the concentration of 5 μM, while the corresponding porphyrins did not. At the concentration of 0.5 μM, the photocytotoxicity increased in the order of **4a** < **4b** < **4c**, which is parallel with the order of the $^1O_2$ quantum yields. In addition, the photocytotoxicity of **4b** and **4c** was significantly inhibited by sodium azide but not D-mannitol, suggesting that $^1O_2$ is the predominant species in the photodynamic action in HeLa cells. Therefore, **4b** and **4c** exhibit the heavy-atom effect in the cellular microenvironment as well as in nonphysiological media. This is a first clear example of an improved systematic cellular response induced by heavy-atom effect of metallochlorin.

Experimental Section

General Information and Materials. All chemicals were of analytical grade. 4′,6-Diamidino-2-phenylindole dihydrochloride hydrate (DAPI) was purchased from Molecular Probes (Eugene, OR). 5,10,15,20-Tetrakis(pentafluorophenyl)porphyrin (**3a**),[34] 5,10,15,20-tetrakis(pentafluorophenyl)porphyrinato palladium(II) (**3b**),[35] 5,10,15,20-tetrakis(pentafluorophenyl)porphyrinato platinum(II) (**3c**),[36] and an azomethine ylide cycloadduct of **3a** (**4a**)[30] were prepared according to the literature. ^1H, ^{13}C, and ^{19}F NMR spectra were recorded using a JNM-AL400 (400 MHz, JEOL Ltd., Tokyo, Japan) instrument. Electronic absorption spectra were recorded on a JASCO V-570 spectrophotometer (JASCO Co., Ltd., Tokyo, Japan). Electron-spray ionization time-of-flight (ESI-TOF) mass spectra were taken on a JEOL JMS-T100LC (JEOL Ltd., Tokyo, Japan). High-resolution mass spectra were obtained using angiotensin I (human) ($C_{62}H_{89}N_{17}O_{14}$, 1295.67749) as an internal standard. Elemental analyses was performed on a Perkin-Elmer 2400 series II CHNS/O elemental analyzer (Perkin-Elmer. Inc., MA). Purity of all compounds tested in vitro was estimated to be >95% by measurement of HPLC using octadecylsilyl-supported silica gel column (Mightysil RP-18 250-4.6 (5 μm), KANTO Chemical Co.) and methanol as an eluent. The morphological changes of the cells were observed using a confocal laser scanning microscope (CLSM) (model LSM 510, Carl Zeiss, Jena, Germany).

Azomethine Ylide Cycloadduct of 3b (4b). 3b (416 mg, 386 μmol), *N*-methylglycine (201 mg, 20.0 mmol), paraformaldehyde (172 mg), and toluene (50 mL) were refluxed for 72 h under N_2. Further *N*-methylglycine (ca. 200 mg) and paraformaldehyde (ca. 170 mg) were added to the mixture 15 times at intervals of 2 h. The solution was washed with distilled water (30 mL × 3), dried over Na_2SO_4, and evaporated under reduced pressure. The crude product was purified by column chromatography (silica gel, $CHCl_3$ to $CHCl_3$:AcOEt = 8:1) and gel permeation chromatography, followed by recrystallization from $CHCl_3$−hexane to give **4b** (75.07 mg, 17.1%) as a blue powder. Purity (HPLC): 96.1%. ^1H NMR (400 MHz, $CDCl_3$, $Si(CH_3)_4$ = 0 ppm): δ (ppm) = 8.44 (4H, d, ^3J = 8.1 Hz, 8,17,12,13-β-pyrrole*H*), 8.16 (2H, d, ^3J = 4.5 Hz, 7,18-β-pyrrole*H*), 5.26 (2H, br, 2,3-β-pyrrole*H*), 3.16 (2H, br, N−C*H*H), 2.53 (2H, br, N-CH*H*), 2.23 (3H, s, N−CH_3). ^{13}C NMR (100 MHz, $CDCl_3$, *C*DCl_3 = 77 ppm): δ (ppm) = 155.90, 145.58, 138.64, 137.88, 131.58, 127.59, 126.92, 108.88, 97.49, 63.58, 50.82, 41.06 and broad peaks due to strong $^{13}C-^{19}F$ coupling were found between 150 and 135 and around 115 ppm. ^{19}F NMR (376 MHz, $CDCl_3$, CF_3CO_2H = −76.05 ppm): δ (ppm) = −135.35 (dd, ^3J = 24.4 Hz, ^5J = 6.1 Hz, 2F, *ortho*-Ph*F*), −137.42 (m, 4F, *ortho*-Ph*F*), −137.73 (dd, ^3J = 24.4 Hz, ^5J = 6.1 Hz, 2F, *ortho*-Ph*F*), −151.71 (t, ^3J = 20.6 Hz, *para*-Ph*F*), −152.11 (t, ^3J = 20.6 Hz, *para*-Ph*F*), −160.45 (m, 2F, *meta*-Ph*F*), −160.84 (m, 2F, *meta*-Ph*F*), −161.73 (m, 4F, *meta*-Ph*F*). ESI-TOF HRMS: *m*/*z* for $C_{47}H_{16}N_5F_{20}Pd$ ($[M + H]^+$) calcd 1136.01212, found 1136.00831 (error −3.81 mmu, −3.35 ppm). Anal. Calcd for $C_{47}H_{15}N_5F_{20}Pd + 0.9C_6H_{14}$: C, 51.86; H, 2.29; N, 5.77. Found: C, 51.44; H, 2.20; N, 5.89. UV−vis ($c = 9.73 \times 10^{-6}$ M, $CHCl_3$, path length = 1 cm, 25 °C): λ/nm ($\varepsilon \times 10^{-3}$/ M^{-1} cm^{-1}) = 603.5 (61.5), 560.5 (9.02), 522.0 (2.60), 490.5 (6.66), 405.5 (132). FL ($c = 1.95 \times 10^{-6}$ M, $CHCl_3$, path length = 1 cm, λ_{ex} = 405.5 nm, 25 °C, N_2): λ/nm = 611, 657, 812.

Azomethine Ylide Cycloadduct of 3c (4c). Compound **3c** (586 mg, 500 μmol), *N*-methylglycine (252 mg, 28.2 mmol), paraformaldehyde (198 mg), and toluene (60 mL) were stirred with N_2 flushing for 20 min. The mixture was refluxed for 72 h under N_2. Further *N*-methylglycine (ca. 250 mg) and paraformaldehyde (ca. 170 mg) were added to the mixture four times at intervals of 2 h. The solution was evaporated under reduced pressure. The residue was poured into $CHCl_3$ (30 mL), washed with distilled water (30 mL × 3), dried over Na_2SO_4, and evaporated under reduced pressure. The crude product was purified by column chromatography (silica gel, $CHCl_3$ to $CHCl_3$:AcOEt = 8:1) and gel permeation chromatography, followed by recrystallization from $CHCl_3$−hexane to give **4c** (78.75 mg, 12.9%) as a blue powder. Purity (HPLC): 96.5%. ^1H NMR (400 MHz, $CDCl_3$, $Si(CH_3)_4$ = 0 ppm): δ (ppm) = 8.47 (4H, br s, 8,17,12,13-β-pyrrole*H*), 8.21 (2H, d, ^3J = 3.1 Hz, 7,18-β-pyrrole*H*), 5.34 (2H, br, 2,3-β-pyrrole*H*), 3.16 (2H, br, N−C*H*H), 2.53 (2H, br, N-CH*H*), 2.23 (3H, s, N−CH_3). ^{13}C NMR (100 MHz, $CDCl_3$, *C*DCl_3 = 77 ppm): δ (ppm) = 155.71, 145.83, 137.17, 135.83, 132.19, 126.95, 125.79, 109.71, 97.63, 63.79, 50.23, 41.01 and broad peaks due to strong $^{13}C-^{19}F$ coupling were found between 150 and 135 and around 115 ppm. ^{19}F NMR (376 MHz, $CDCl_3$, CF_3CO_2H = −76.05 ppm): δ (ppm) = −135.27 (dd, ^3J = 24.4 Hz, ^5J = 7.6 Hz, 2F, *ortho*-Ph*F*), −137.35 (m, 4F, *ortho*-Ph*F*), −137.62 (dd, ^3J = 23.6 Hz, ^5J = 6.9 Hz, 2F, *ortho*-Ph*F*), −151.53 (t, ^3J = 20.6 Hz, *para*-Ph*F*), −151.96 (t, ^3J = 20.6 Hz, *para*-Ph*F*), −160.32 (m, 2F, *meta*-Ph*F*), −160.72 (m, 2F, *meta*-Ph*F*), −161.59 (m, 4F, *meta*-Ph*F*). ESI-TOF HRMS: *m*/*z* for $C_{47}H_{16}N_5F_{20}Pt$ ($[M + H]^+$) calcd 1225.07341, found 1225.07378 (error 0.37 mmu, 0.30 ppm). Anal. Calcd for $C_{47}H_{15}N_5F_{20}Pt + 0.5C_6H_{14}$: C, 47.37; H, 1.75; N, 5.52. Found: C, 47.79; H, 1.99; N, 5.50. UV−vis ($c = 11.5 \times 10^{-6}$ M, $CHCl_3$, path length = 1 cm, 25 °C): λ/nm ($\varepsilon \times 10^{-3}$/$M^{-1}$ cm^{-1}) = 595.5 (58.0), 557.0 (9.33), 509.5 (2.86), 478.0 (6.03), 394.5 (147). FL ($c = 1.15 \times 10^{-6}$ M, $CHCl_3$, path length = 1 cm, λ_{ex} = 394.5 nm, 25 °C, N_2): λ/nm = 604, 657, 786.

X-Ray Structural Determination. Single crystal X-ray diffraction data were recorded on Rigaku Mercury CCD and AFC/Mercury CCD diffractometers using graphite-monochromated Mo Kα radiation. All data sets were corrected for Lorentzian polarization effects and for absorption. All structures were solved by the direct method (SIR97[49]). Hydrogen atoms were placed into calculated positions and refined with isotropic thermal parameters riding on those of the parent atoms. Refinement of the non-hydrogen atoms was carried out with the full-matrix least-squares technique.

$^1O_2$ Luminescence Measurement. An air-saturated C_6D_6 solution of a sample (the absorbance of the solution was adjusted to be 0.2 at 532 nm) in a quartz cell (optical path length 10 mm) was excited at 532 nm using a Cosmo System LVU-200S spectrometer. Near-IR emission spectra of singlet oxygen were recorded on a SPEX Fluorolog τ3 fluorescence spectrophotometer. A photomul-

tiplier (Hamamatsu Photonics, R5509-72) was used to detect emission in the near-infrared region.

Photocytotoxicity Test. HeLa cells (ATCC CCL-2) were obtained from Dainippon-Sumitomo Pharmaceutical (Osaka, Japan). They were grown in Dulbecco's modified Eagle's medium (DMEM) containing 10% fetal calf serum (FCS) (Hyclone Laboratories, Inc., Logan, UT). The photocytotoxicity of photosensitizers and TPPS in HeLa cells was examined as follows: HeLa cells (5×10^3 cells) in 100 μL of DMEM containing 10% FCS were plated in a 96-well plate (Nalge Nunc International, Naperville, IL) and incubated for 24 h (37 °C, 5% CO_2). Then 100 μL of a photosensitizer in DMEM containing 10% FCS and 2% DMSO was added to each well. Incubation was carried out for 24 h at a photosensitizer concentration of 0.5 or 5 μM (final DMSO content was 1% in all cases). The cells were washed twice with phosphate-buffered saline (PBS), and then 100 μL of DMEM containing 10% FCS was added. The cells were exposed to light from a 100 W halogen lamp (KBEX-102A, USHIO Inc., Tokyo, Japan), equipped with a water jacket, and a Y-50 cutoff filter ($\lambda > 500$ nm, Toshiba Co., Tokyo, Japan). The light intensity was adjusted by using a UV−vis power meter (ORION/TH Ophir Optronics Ltd., Jerusalem, Israel). The light dose was calculated as the product of light intensity ($mW \cdot cm^{-2}$) and irradiation time, and the irradiation time was adjusted to obtain the desired light dose of 16 $J \cdot cm^{-2}$. Cell viability was measured after 24 h using WST-8 reagent (10 μL) from Cell Counting Kit-8 (Dojindo, Tokyo, Japan) according to the manufacturer's instructions. The percentage cell survival was calculated by normalization with respect to the value for no drug treatment.

Photocytotoxicity Test with ROS Inhibitor. HeLa cells (5×10^3 cells) in 100 μL of DMEM containing 10% FCS were plated in a 96-well plate and incubated for 24 h (37 °C, 5% CO_2). Then 100 μL of a photosensitizer in DMEM containing 10% FCS and 2% DMSO was added to each well. Incubation was then continued for 24 h in the presence of the photosensitizer. The photosensitizer concentration was 0.8 μM for **4a** and 0.4 μM for **4b** and **4c** in DMEM containing 10% FCS (the final concentration of DMSO was 1% in all cases). The cells were washed twice with PBS, and then 100 μL of DMEM containing 10% FCS (control) or 100 μL of ROS quencher (1 or 5 mM NaN_3 as a singlet oxygen quencher; 4 or 40 mM D-mannitol as a hydroxyl radical scavenger) in DMEM containing 10% FCS was added. The cells were incubated for 2 h (37 °C, 5% CO_2) and then exposed to light under the same conditions as described in the previous section. After 30 min of photoirradiation, the medium was replaced with fresh medium. The percentage cell survival was determined by means of the same protocol as described in the previous section.

Confocal Laser-Scanning Microscopy. HeLa cells (3×10^4 cells) in 500 μL of DMEM containing 10% FCS were plated in two 24-well plates (Nalge Nunc International, Naperville, IL) and incubated for 24 h (37 °C, 5% CO_2). Then 500 μL of 1.0 μM **4c** in DMEM containing 10% FCS and 2% DMSO was added to each well, and incubation was continued for 24 h in the presence of the photosensitizers. The final concentration of photosensitizers was 0.5 μM (1% DMSO). The cells in one 24-well plate were washed twice with 500 μL of PBS, and 500 μL of Hank's balanced salt solution (HBSS) was added to each well. Fluorescence images of photosensitizers in cells were taken with a confocal laser scanning microscope (CLSM) (LSM510, Carl Zeiss) using an excitation wavelength of 543 nm (photosensitizers) or 364 nm (nuclear/DAPI). For the other plate, 500 μL of DMEM containing 10% FCS was added to each well instead of HBSS. Then the plate was photoirradiated under the same conditions as described in the previous section. After 20 h of photoirradiation, the cells were stained with 4′,6-diamidino-2-phenylindole dihydrochloride hydrate (DAPI) 0.3 μM for 5 min at room temperature and then washed twice with 500 μL of PBS, and finally 500 μL of HBSS was added. Fluorescence images of DAPI-stained cells were taken using an excitation wavelength of 364 nm.

Statistical Analysis. All statistical evaluations were performed using Student's *t*-test. All values for cellular uptake and cytotoxicity are expressed as mean ± standard deviation.

Acknowledgment. This work was supported by a Grants-in-Aid for Scientific Research from the Ministry of Education, Culture, Sport, Science and Technology (MEXT) of the Japanese Government, a Nara Women's University Intramural Grant for Project Research, and grants from the Kao Foundation for Arts and Sciences, the NAIST Presidential Special Fund, Japan−German exchange program supported by Japan Society for the Promotion of Science (JSPS), and REI MEDICAL Foundation.

Supporting Information Available: Analytical data of compounds tested, crystal and spectral data of **4b** and **4c** in PDF file; X-ray crystallographic files of **4b** and **4c**. This material is available free of charge via the Internet at http://pubs.acs.org.

References

(1) Detty, M. R.; Gibson, S. L.; Wagner, S. J. Current clinical and preclinical photosensitizers for use in photodynamic therapy. *J. Med. Chem.* **2004**, *47*, 3897–3915.
(2) Nyman, E. S.; Hynninen, P. H. Research advances in the use of tetrapyrrolic photosensitizers for photodynamic therapy. *J. Photochem. Photobiol., B* **2004**, *73*, 1–28.
(3) Kessel, D. Photodynamic therapy: from the beginning. *Photodiagn. Photodyn. Ther.* **2004**, *1*, 3–7.
(4) MacDonald, I. J.; Dougherty, T. Basics principles of photodynamic therapy. *J. Porphyrins Phthalocyanines* **2001**, *5*, 105–129.
(5) Pandey, R. K. Recent advances in photodynamic therapy. *J. Porphyrins Phthalocyanines* **2000**, *4*, 368–373.
(6) Bonnet, R. *Chemical Aspects of Photodynamic Therapy*; Gordon and Breach Science Publishers: The Netherlands, 2000.
(7) Castano, A. P.; Demidova, T. N.; Hamblin, M. R. Mechanism in photodynamic therapy, part one: photosensitizers, photochemistry and cellular localization. *Photodiagn. Photodyn. Ther.* **2004**, *1*, 279–293.
(8) Castano, A. P.; Demidova, T. N.; Hamblin, M. R. Mechanism in photodynamic therapy, part two: cellular signaling, cell metabolism and modes of cell death. *Photodiagn. Photodyn. Ther.* **2005**, *2*, 1–23.
(9) Castano, A. P.; Demidova, T. N.; Hamblin, M. R. Mechanism in photodynamic therapy, part three: photosensitizer pharmacokinetics, biodistribution, tumor localization and modes of tumor destruction. *Photodiagn. Photodyn. Ther.* **2005**, *2*, 91–106.
(10) McGlynn, S. P.; Azumi, T.; Kinoshita, M. *Molecular Spectroscopy of the Triplet State*; Prentice-Hall: Englewood Cliffs, NJ, 1969.
(11) Fukuzumi, S.; Ohkubo, K.; Zheng, X.; Chen, Y.; Pandey, R.; Zhan, R.; Kadish, K. M. Metal bacteriochlorins which act as dual singlet oxygen and superoxide generators. *J. Phys. Chem. B* **2008**, *112*, 2738–2746.
(12) Henderson, B. W.; Sumlin, A. B.; Owczarczak, B. L.; Dougherty, T. J. Bacteriochlorophyll-*a* as photosensitizer for photodynamic treatment of transplantable murine tumors. *J. Photochem. Photobiol., B* **1991**, *10*, 303–313.
(13) Rosenbach-Belkin, V.; Chen, L.; Fiedor, L.; Tregub, I.; Pavlotsky, F.; Brumfeld, V.; Salomon, Y.; Scherz, A. Serine conjugates of chlorophyll and bacteriochlorophyll: photocytotoxicity in vitro and tissue distribution in mice bearing melanoma tumors. *Photochem. Photobiol.* **1996**, *64*, 174–181.
(14) Ziberstein, J.; Schreiber, S.; Bloemers, M. C. W. M.; Bendel, P.; Neeman, M.; Schechtman, E.; Kohen, F.; Scherz, A.; Salomon, Y. Antivascular treatment of solid melanoma tumors with bacteriochlorophyll-serine-based photodynamic therapy. *Photochem. Photobiol.* **2001**, *73*, 257–266.
(15) Kelleher, D. K.; Thews, O.; Scherz, A.; Salomon, Y.; Vaupel, P. Combined hyperthermia and chlorophyll-based photodynamic therapy: tumor growth and metabolic microenvironment. *Br. J. Cancer* **2003**, *89*, 2333–2339.
(16) Kozyrev, A. N.; Chen, Y.; Goswami, L. N.; Tabaczynski, W. A.; Pandey, R. K. Characterization of porphyrins, chlorins, and bacteriochlorins formed via allomerization of bacteriochlorophyll a. Synthesis of highly stable bacteriopurprinimides and their metal complexes. *J. Org. Chem.* **2006**, *71*, 1949–1960.
(17) Chen, Q.; Huang, Z.; Luck, D.; Beckers, J.; Brun, P. H.; Wilson, B. C.; Scherz, A.; Salomon, Y.; Hetzel, F. W. Preclinical studies in normal canine prostate of a novel palladium-bacteriopheophorbide (WST09) photosensitizer for photodynamic therapy of prostate cancers. *Photochem. Photobiol.* **2002**, *76*, 438–445.
(18) Vakrat-Haglili, Y.; Weiner, L.; Brumfeld, V.; Brandis, A.; Salomon, Y.; Mcllroy, B.; Wilson, B. C.; Pawlak, A.; Rozanowska, M.; Sarna, T.; Scherz, A. The microenvironment effect on the generation of reactive oxygen species by Pd-bacteriopheophorbide. *J. Am. Chem. Soc.* **2005**, *127*, 6487–6497.
(19) Pogue, B. W.; Redmond, R. W.; Trivedi, N.; Hasan, T. Photophysical properties of tin ethyl etiopurpurin I ($SnEt_2$) and tin octaethylben-

zochlorin (SnOEBC) in solution and bound to albumin. *Photochem. Photobiol.* **1998**, *68*, 809–815.
(20) Stolzenberg, A. M.; Strauss, S. H.; Holm, R. H. Iron(II, III)−chlorin and−isobacteriochlorin complexes. Models of the heme prosthetic groups in nitrite and sulfite reductases: Means of formation and spectroscopic and redox properties. *J. Am. Chem. Soc.* **1981**, *103*, 4763–4778.
(21) Stolzenberg, A. M.; Schussel, L. J. Synthesis, characterization, and electrochemistry of copper(II) and palladium(II) hydrochlorins: The copper(I) octaethylisobacteriochlorin anion. *Inorg. Chem.* **1991**, *30*, 3205–3213.
(22) Stolzenberg, A. M.; Stershic, M. T. Oxidative chemistry of nickel hydroporphyrins. *Inorg. Chem.* **1988**, *27*, 1614–1620.
(23) Singh, A.; Huang, W.-Y.; Wgbujor, R.; Johnson, L. W. Single site electronic spectroscopy of zinc and magnesium chlorin in *n*-octane matrixes at 7 K. *J. Phys. Chem. A* **2001**, *105*, 5778–5784.
(24) Zenkevich, E.; Sagun, E.; Knyukshto, V.; Shulga, A.; Mironov, A.; Efremova, O.; Bonnett, R.; Songca, S. P.; Kassem, M. Photophysical and photochemical properties of potential porphyrin and chlorin photosensitizers for PDT. *J. Photochem. Photobiol., B* **1996**, *33*, 171–180.
(25) Leonard, K. A.; Nelen, M. I.; Anderson, L. T.; Gibson, S. L.; Hilf, R.; Detty, M. R. 2,4,6-Triarylchalcogenopyrylium dyes related in structure to the antitumor agent AA1 as in vitro sensitizers for the photodynamic therapy of cancer. *J. Med. Chem.* **1999**, *42*, 3942.
(26) Azenha, E. G.; Serra, A. C.; Pineiro, M.; Pereira, M. M.; de Melo, J. S.; Arnaut, L. G.; Formosinho, S. J.; Rocha Gonsalves, A M. d'A. Heavy-atom effect on metalloporphyrins and polyhalogenated porphyrins. *Chem. Phys.* **2002**, *280*, 177–190.
(27) Scalise, I.; Durantini, E. N. Photodynamic effect of metallo 5-(4-carboxypheny)-10,15,20-tris(4-methylphenyl) porphyrins in biomimetic AOT reverse micelles containing urease. *J. Photochem. Photobiol., A* **2004**, *162*, 105–113.
(28) Serra, C. A.; Pineiro, M.; Rocha Gonsalves, A. M. d'A.; Abrantes, M.; Laranjo, M.; Santos, A. C.; Botelho, M. F. Halogen atom effect on photophysical and photodynamic characteristics of derivatives of 5,10,15,20-tetrakis(3-hydroxyphenyl)porphyrin. *J. Photochem. Photobiol., B* **2008**, *92*, 59–65.
(29) Gorman, A.; Killoran, J.; O'Shea, C.; Kenna, T.; Gallagher, W. M.; O'Shea, D. F. In vitro demonstration of the heavy-atom effect for photodynamic therapy. *J. Am. Chem. Soc.* **2004**, *126*, 10619–10631.
(30) Silva, A. M. G.; Tomé, A. C.; Neves, M. G. P. M. S.; Silva, A. M. S.; Cavaleiro, J. A. S. 1,3-Dipolar cycloaddition reactions of porphyrins with azomethine ylides. *J. Org. Chem.* **2005**, *70*, 2306–2314.
(31) Silva, A. M. G.; Lacerda, P. S. S.; Tomé, A. C.; Neves, M. G. P. M. S.; Silva, A. M. S.; Cavaleiro, J. A. S.; Makarova, E. A.; Lukyanets, E. A. Porphyrins in 1,3-dipolar cycloaddition reactions. synthesis of new porphyrin−chlorin and porphyrin−tetraazachlorin dyads. *J. Org. Chem.* **2006**, *71*, 8352–8356.
(32) Gałęzowski, M.; Gryko, D. T. Synthesis of locked *meso*-β-substituted chlorins via 1,3-dipolar cycloaddition. *J. Org. Chem.* **2006**, *71*, 5942–5950.
(33) Recently Vinhado et al. have synthesized Mn(III) complexes of H_2TFPC by metal insertion into H_2TFPC. Vinhado, F. S.; Gandini, M. E. F.; Iamamoto, Y.; Silva, A. M. G.; Simões, M. M. Q.; Neves, M. G. P. M. S.; Tomé, A. C.; Rebelo, S. L. H.; Pereira, A. M. V. M.; Cavaleiro, J. A. S. Novel Mn(III)chlorins as versatile catalysts for oxyfunctionalisation of hydrocarbons under homogeneous conditions. *J. Mol. Catal. A: Chem.* **2005**, *239*, 138–143.
(34) Kashiwagi, Y.; Imahori, H.; Araki, Y.; Ito, O.; Yamada, K.; Sakata, Y.; Fukuzumi, S. Strong inhibition of singlet oxygen sensitization in pyridylferrocene-fluorinated zinc porphyrin supramolecular complexes. *J. Phys. Chem. A* **2003**, *107*, 5515–5522.
(35) Spellane, P. J.; Gouterman, M.; Antipas, A.; Kim, S.; Liu, Y. C. Porphyrin. 40. Electronic spectra and four-orbital energies of free-base, zinc, copper, and palladium tetrakis(perfluorophenyl)porphyrins. *Inorg. Chem.* **1980**, *19*, 386–391.
(36) Che, C.-M.; Hou, Y.-J.; Chan, M. C. W.; Guo, J.; Liu, Y.; Wang, Y. *meso*-Tetrakis(pentafluorophenyl)porphyrinato]platinum(II) as an efficient, oxidation-resistant red phosphor: spectroscopic properties and applications in organic light-emitting diodes. *J. Mater. Chem.* **2003**, *13*, 1362–1366.
(37) Pandey, S. K.; Gryshuk, A. L.; Graham, A.; Ohkubo, K.; Fukuzumi, S.; Dobhal, M. P.; Zheng, G.; Ou, Z.; Zhan, R.; Kadish, K. M.; Oseroff, A.; Ramaprasade, S.; Pandey, R. K. Fluorinated photosensitizers: synthesis, photophysical, electrochemical, intracellular localization, in vitro photosensitizing efficacy and determination of tumor-uptake by ^{19}F in vivo NMR spectroscopy. *Tetrahedron* **2003**, *59*, 10059–10073.
(38) Spaulding, L. D.; Andrews, L. C.; Williams, G. J. B. Crystal and molecular structure of 2,3-dihydro-$\alpha,\beta,\gamma,\delta$-tetraphenylporphyrinato-pyridinezinc(II)-benzene solvate. *J. Am. Chem. Soc.* **1977**, *99*, 6918–6923.
(39) Barkigia, K. M.; Fajer, J.; Spaulding, L. D.; Williams, G. J. B. Crystal and molecular structure of the isobacteriochlorin: (2,3,7,8-tetrahydro-5,10,15,20-tetraphenylporphinato)(pyridine)zinc(II) benzene solvate. *J. Am. Chem. Soc.* **1981**, *103*, 176–181.
(40) Strauss, S. H.; Silver, M. E.; Long, K. M.; Thompson, R. G.; Hudgens, R. A.; Spartalian, K.; Ibers, J. A. Comparison of the molecular and electronic structure of (2,3,7,8,12,13,17,18-octaethylporphyrinato)iron(II) and (*trans*-7,8-dihydro-2,3,7,8,12,13,17,18-octaethylporphyrinato)iron(II). *J. Am. Chem. Soc.* **1985**, *107*, 4207–4215.
(41) Ulman, A.; Gallucci, J.; Fisher, D.; Ibers, J. A. Facile syntheses of tetraalkylchlorin and tetraalkylporphyrin complexes and comparison of the structures of the tetramethylchlorin and tetramethylporphyrin complexes of nickel(II). *J. Am. Chem. Soc.* **1980**, *102*, 6852–6854.
(42) Suk, M. P.; Swepston, P. N.; Ibers, J. A. Direct preparation of a siroheme model compound: synthesis and structure of (5,10,15,20-tetramethylisobacteriochlorinato)nickel(II). *J. Am. Chem. Soc.* **1984**, *106*, 5164–5171.
(43) Stolzenberg, A. M.; Schussel, L. J.; Summers, J. S.; Foxman, B. M.; Petersen, J. L. Structures of the homologous series of square-planar metallotetrapyrroles palladium(II) octaethylporphyrin, palladium(II) *trans*-octaethylchlorin, and palladium(II) *tct*-octaethylisobacteriochlorin. *Inorg. Chem.* **1992**, *31*, 1678–1686.
(44) Drain, C. M.; Gentemann, S.; Roberts, J. A.; Nelson, N. Y.; Medforth, C. J.; Jia, S.; Simpson, M. C.; Smith, K. M.; Fajer, J.; Shelnutt, J. A.; Holten, D. Picosecond to microsecond photodynamics of a nonplanar nickel porphyrin: solvent dielectric and temperature effects. *J. Am. Chem. Soc.* **1998**, *120*, 3781–3791.
(45) Singh, A.; Johnson, L. W. Phosphorescence spectra and triplet state lifetimes of palladium octaethylporphyrin, palladium octaethylchlorin and palladium 2,3-dimethyloctaethylisobacteriochlorin at 77 K. *Spectrochim. Acta, Part A* **2003**, *59*, 905–908.
(46) Thalladi, V. R.; Weiss, H.-C.; Bläser, D.; Boese, R.; Nangia, A.; Desiraju, G. R. C−H···F Interaction in the crystal structures of some fluorobenzenes. *J. Am. Chem. Soc.* **1998**, *120*, 8702–8710.
(47) Abogast, J. W.; Darmanyan, A. P.; Chrostopher, P. D.; Foote, C. S.; Rubin, Y.; Diederich, F. N.; Alvarez, M. M.; Anz, S. J.; Whetten, R. L. Photophysical properties of C_{60}. *J. Phys. Chem.* **1991**, *95*, 11–12.
(48) Ding, X.; Xu, Q.; Liu, F.; Zhou, P.; Gu, Y.; Zeng, J.; An, J.; Dai, W.; Li, X. Hematoporphyrin monomethyl ether photodynamic damage on HeLa cells by means of reactive oxygen species production and cytosolic free calcium concentration elevation. *Cancer Lett.* **2004**, *216*, 43–54.
(49) Altomare, A.; Burla, M. C.; Camalli, M.; Cascarano, G. L.; Carmelo Giacovazzo, C.; Guagliardi, A.; Moliterni, A. G. G.; Polidori, G.; Riccardo Spagna, R. SIR97: a new tool for crystal structure determination and refinement. *J. Appl. Crystallogr.* **1999**, *32*, 115–119.

JM8015427